Flowability of granular materials in a rotating drum: Investigation of relevant flow descriptors

Reem Khazem, Julien Colin, Joel Casalinho, John Pachón-Morales, François Puel

This Accepted author version was available online 2025, 9th of June.

To cite this article: **R. Khazem, J. Colin, J. Casalinho, et al., Flowability of granular materials in a rotating drum: Investigation of relevant flow descriptors, *Powder Technology* 464 (2025), 121231** https://doi.org/10.1016/j.powtec.2025.121231

Flowability of granular materials in a rotating drum: investigation of relevant flow descriptors

Reem KHAZEM[a,*], Julien COLIN[a,b], Joel CASALINHO[a], John PACHÓN-MORALES [c], and François PUEL[a]

[a] *Université Paris-Saclay, CentraleSupélec, Laboratoire de Génie des Procédés et Matériaux, 91190, Gif-sur-Yvette, France*
[b] *Université de Lorraine, Laboratoire Réactions et Génie des Procédés, CNRS, 54000, Nancy, France*
[c] *Campus d'Innovation Air Liquide, 78350, Les Loges-en-Josas, France*

ABSTRACT

The characterization of granular material flowability is highly significant for recognizing the complex dynamic behavior of particulate matter in a wide range of industrial processes. Flows can be categorized into confined and unconfined types. While a universal standard exists for assessing flowability in confined state, defined by the Flow Function Coefficient (FFC) obtained from a ring shear tester, there is currently no established standard for assessing flowability in unconfined state. This research aims at evaluating the performance of some descriptors in distinguishing diversity of flow behaviors of several materials, having distinct properties, in unconfined state using an in-house rotating drum coupled with image processing. A rigorous experimental method was developed to ensure reproducibility and accuracy in results obtained with the different material that show a wide diversity in behaviors. Different flowability descriptors were calculated after image processing using MATLAB based on the average value and the standard deviation of irregularity of the surface profile (r^2), the angle of repose (θ), the centroid angle (β), the projected area (A), and of the profile peak (y_{max}), and finally, the cohesive index (CI). The mentioned standard deviation is linked to the range of fluctuations level of the data during rotation. From the application of these descriptors to the recorded flows, the potential of this approach to distinguish the powders behaviors is validated. These outcomes will enhance the understanding of powder behavior under low-stress conditions, aiding process optimization.

Keywords:

Cohesive and non-cohesive powder, Unconfined state, Image processing, Cohesive index, Centroid angle, Angle of repose, Irregularity of the surface profile

1 Introduction

Powders are commonly used in industry that requires to process raw materials in solid phase, such as pharmaceuticals, food processing, and chemical manufacturing. Powder flow, also referred to as

flowability, is defined as the relative movement of a bulk of particles among adjacent particles or along the walls [1]. This is an important property of granular materials as it influences many industrial processes, since flowability can either improve or impair the efficiencies of material handling, transport, and storage [2–4] and lead to increased operational costs. Poor flowability can lead to bridging, uneven dosing, and segregation.

For granular materials, flowability is a challenging property to quantify. A given granular material can behave differently depending on the operating condition. Therefore, there is a wide variety of flow characterization techniques available in the literature [5], especially depending on the powder state – confined or unconfined–. The flowability of a powder in confined state can be determined through various standard methods, such as Jenike's method (*ASTM D6128-22*) and the Schulze's method (*ASTM D6773-22*) [5,6]. Both methods are applicable from not flowing to free flowing powders, that can be compared via their respective value of Flow Function Coefficient (FFC) and flowability classes are established: not flowing (FFC<1), very cohesive powders (1<FFC<2), cohesive (2<FFC<4), easy flowing (4<FFC<10), and free-flowing (FFC<10) [7]. These methods are valid as an engineering tool addressing powder in a defined confined state, for example for designing storage facilities. On the other hand, the flowability in unconfined state determines the powder behavior under low stress conditions, when the powders are transferred from one container to another, fed into machines, or mixed with other powders.

One of the most potent techniques to study the flowability of unconfined powders is the rotating drum technique. The powder samples inside the drum only experience stress mainly from gravity acting on their own mass. It is thus a relevant method to foresee the behavior of a powder in a pipe or being handled by a conveying screw. The potential of powder avalanching assessment to determine the effect of an added ingredient on the rheology of a powdered mixture was first investigated by Kaye et al. [8] more than one decade ago. Hung et al. presented later a theoretical framework to predict and explain the transition between different granular flow regimes in rotating drums [9]. Since then, the interest in rotating drums for flowability characterization has grown steadily, but there's still no standardized universal norm to be followed. This method involves a cylindrical drum partially filled with powder, rotating at a controlled speed [10]. During the experiment, the 2D-movement of the powder –in the cylinder section– is grabbed thanks to a high-speed camera. Flow characteristics are determined through image processing.

Several flowability descriptors are used to characterize how granular materials behave. Authors have not systematically indicated the reason for the choice of descriptor, but it might depend on the characteristics of the material being studied, the application requirements, and mostly the experimental setup capabilities. Through literature review, flowability descriptors could be classified into categories based on the bulk of the powder and its free-surface, that can be analyzed in different ways: energy content of powder [11–13], events frequency and duration [14,15], powder profile (powder-air interface) [10,16–20], and projection area of powder bulk [18,21,22]. Some of these descriptors are applied in this study, others are improved, and new ones are introduced.

The aim of this study is to evaluate the performance of each of these descriptors in distinguishing the diversity of flow behavior of different granular materials in the unconfined state, ranging from poorly to highly cohesive. This paper does not investigate the microscopic interactions between particles which govern the flowability, but instead remains at a macroscopic level using descriptors.

2 Materials and methods

2.1 Granular materials

Different granular materials were selected to allow the investigation of a broad range of flow characteristics. This diversity of behaviors arises from variations in grain size and shape (spherical *vs*. elongated), as well as differences in composition (organic *vs*. inorganic) and density [4,23].

The inorganic granular materials are 0.5 mm diameter glass beads, zinc powder (*Thermo Scientific,* CAS: 7440-66-6, *97 % purity*) and sand (*Fisher Chemical,* CAS: 14808-60-7 *low iron*). Biomass powders were produced in laboratory from softwood (*Picea abies*, 450 kg/m^3, cut from a 73-year-old tree grown in the forest in the Auvergne region, France) and hardwood (*Populus euroamericana* 'Koster', 364 kg/m^3, cut from a 25-year-old tree grown in the forest in La Suippe Valley in la Marne, France). For preparing these powders, dry wood boards of both species were first cut into chips of size 60×80×15 mm^3. All chips were ground using a cutting mill (*Retsch, SM300*) with blades rotating at 1500 rpm and a bottom sieve of 1 mm trapezoid holes at the outlet.

The particle size and the bulk density of the different granular materials are presented in **Table 1**. The bulk density was determined through the following consistent procedure. Prior to sampling, the granular materials were mixed with a spatula to ensure homogeneity. A 62.83 cm³ sample (40 % of the drum volume) was then collected by filling cylindrical container, without settling, and its mass was measured.

Table 1: Summary of the used materials

Granular material	Size	Bulk density (g/cm^3)
Glass beads	0.5 mm mean diameter [a]	1.63 (± 0.002)
Zinc powder	100 mesh [b]	3.04 (± 0.010)
Sand	40 - 100 mesh [b]	1.49 (± 0.007)
Spruce powder	< 1 mm sieve cut [c]	0.14 (± 0.004)
Poplar powder	< 1 mm sieve cut [c]	0.21 (± 0.005)

a: measured using a *Sympatec-QICPIC*® morphological particle size analyzer *b*: information from supplier *c*: size of the grid used in the mill

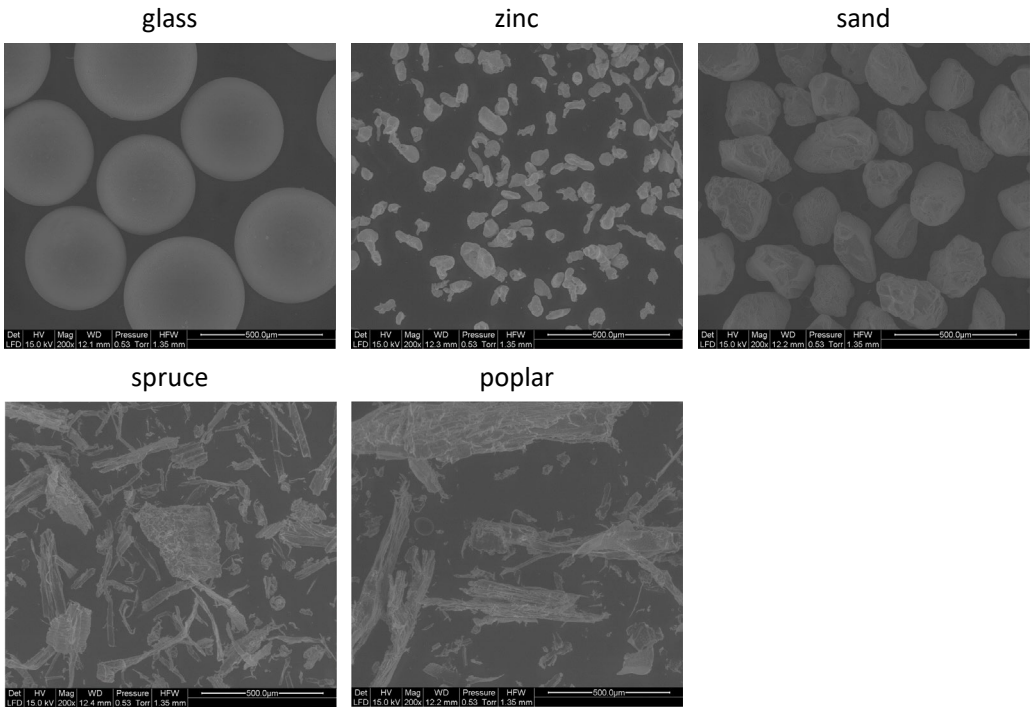

Fig. 1. SEM images of the different granular materials.

2.2 Experimental set-up

The design of the rotating drum must ensure that no external disturbances may perturb the granular materials motion when studying their flow behavior such as mechanical vibrations, bad wheeling and inadequate sealing allowing the penetration of air or dust into the cylinder [24]. Thus, a custom experimental device was developed to analyze the dynamic behaviors over a wide range of rotational speeds. The device was specifically designed to meet several key objectives such as (i) Consistent and smooth rotation to prevent any perturbation of the intrinsic powder behavior, (ii) Good lighting quality to allow accurate and easy post-processing of images, (iii) partial dissipation of electrical charges to reduce the impact of electrostatic forces, (iv) appropriate range of rotational speeds (v) easy sample repositioning without optical or mechanical perturbation.

The core component of this device is a stainless-steel cylinder (10 cm inner diameter, 2 cm width and inner roughness Ra ≈ 0.4 µm) as shown in **Fig. 2**. The cylinder diameter is wide enough to limit edge effects on the granular material and its depth is narrow enough to be able to capture a representative profile shape by image recording. Two transparent conductive glass discs coated with indium-tin oxide are used to improve the drainage of static electricity and to limit the adhesion of grains on these glass discs. The drum is clamped in a roller bearing (*IKO*, *NAG 4924UU*, double roller row and 45 mm width). The drive mechanism is composed of a motor (*Maxon, RE040G/PM52,* brushless, 150 W) and two pulleys (one exchangeable) connected by a toothed belt, resulting in stable and accurate rotational speed variable between 0.01 rpm to 73 rpm depending on the pulley-belt configuration. The design ensures a regular and smooth rotation without vibrations. In this work, the rotational speed is fixed to study the relevance of different flow descriptors rather than the impact of the rotational speed on the powder flow. The need was to choose a rotational speed which allows observing clear and comparable flow regimes ranging from sliding to cascading for all the presented

granular materials [25]. After several tests, preliminary results confirmed that 1 rpm is a convenient choice.

The filling ratio is a critical factor which can also affect the granular material flow, especially its behavior upon avalanching [26]. According to J. Mellmann [25], the filling ratio determines the degree of the interaction between particles –depending on space available for the particles to move– and the thus flow regime. Considering the different granular material used, a filling ratio of 40 % (63 cm^3) of the cylinder volume was used in this work as a compromise between ensuring adequate particle interaction and avoiding excessive clumping. Special care was taken on the mechanical design in order to ensure an easy re-filling/repositioning of the drum.

A high-speed camera (*Photron, FASTCAM Mini AX100*, maximum resolution 1024x1024 pixels, maximum frame rate 4000 fps) and a lens (SIGMA, *EX DG Macro OS,* 105 mm, f2.8) were used to record powder motion. An optical bench ensures axial alignment between center of view of the camera and the drum's rotation axis. In order to ensure a uniform lighting and to create high-contrast shadow images of the powder, a LED lighting panel (*PHLOX, LEDWBL,* 200x200 mm^2, 24 V*)* was mounted behind the drum (regarding to the camera). The camera settings were chosen to have a framerate of 50 fps, resolution of 1024×1024 pixels, and 1/60000 s exposure time. This configuration enables taking unblurred images all along the flow, even when avalanches occur, and allows recording non-saturated images. The original images are in TIFF format with a 12-bit depth. Preliminary tests showed that a stabilization period of the camera CCD was necessary before recording images as the images gray scale values were initially alternating. Thus, the camera and light were switched on 2 hours before the experiment beginning. For each test, 10918 images were recorded during 3.6 min.

At the beginning of the experiment, a time-dependent behavior of the granular material show that a transient period occurs before a quasi-static regime is reached. To ensure the relevance of the comparison between different granular materials, the study of their behavior must be carried out in a quasi-static regime. The longest transient regime that has been observed lasted 2 minutes. To exclude the transient regime from the recording, the drum rotates from the beginning of the camera-light's 2-hour stabilization period.

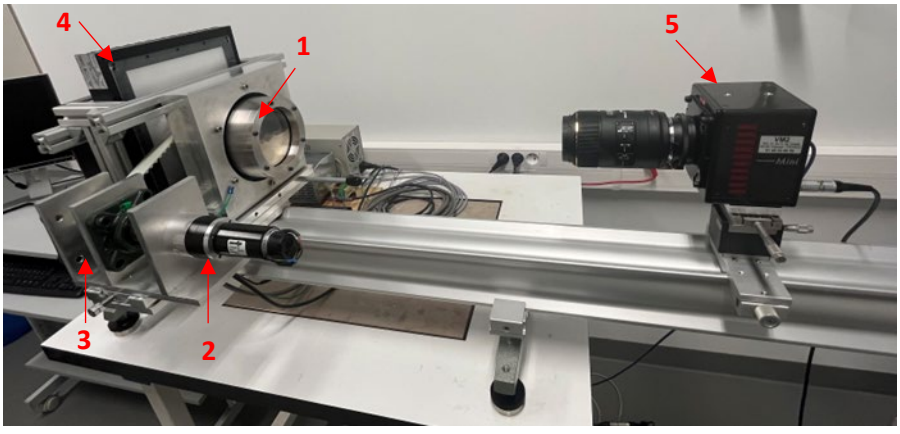

Fig. 2. Rotating drum system: 1: rotating cylinder, 2: motor, 3: drive system, 4: lighting panel, 5: high-speed camera.

2.3 Image Post-Processing

A MATLAB code was developed to automatically process images and obtain the granular bed profiles over time. The procedure was implemented using the Image Processing Toolbox™, and the general sequence of the algorithm is summarized as a flowchart in **Fig. 3**.

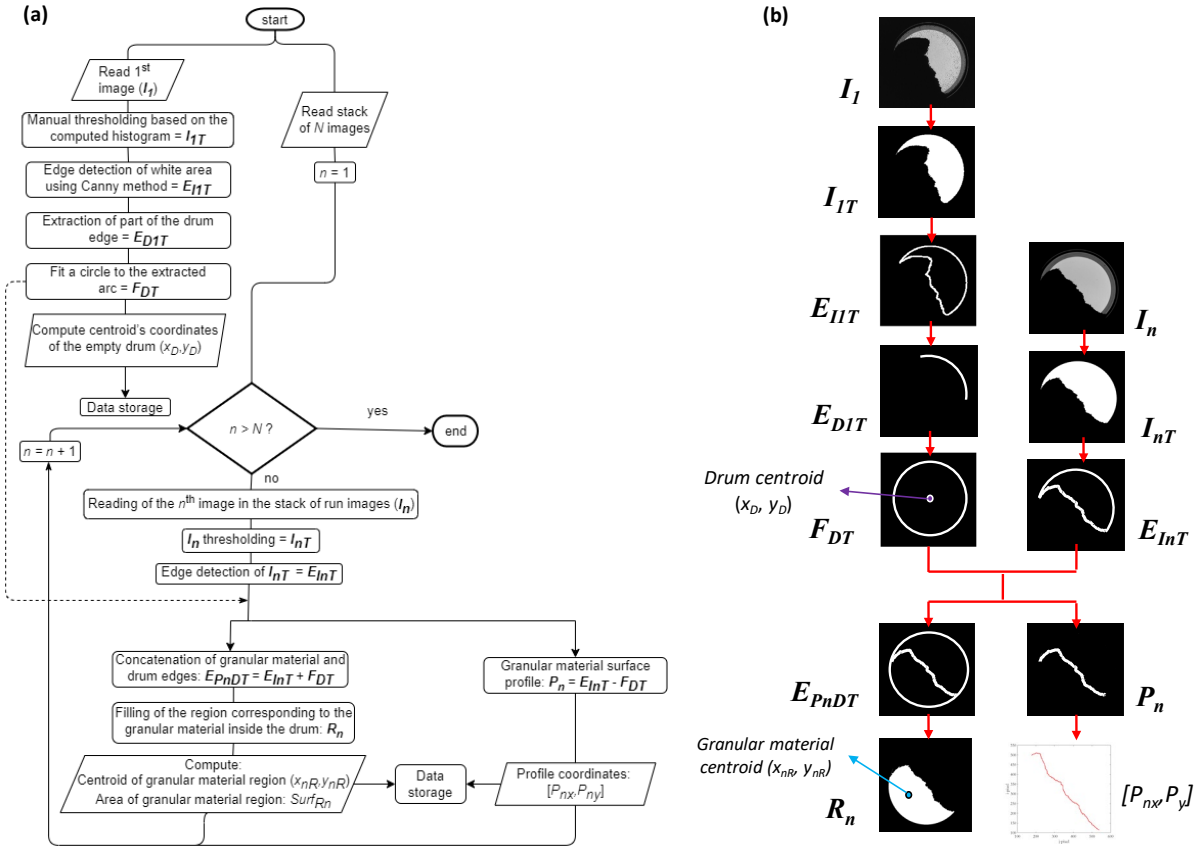

Fig. 3. (a) Image processing flowchart. (b) Main stages of image processing.

The image processing procedure involves four main steps: (*i*) identify the drum circumference – from step I_1 to F_{DT} –, (*ii*) identify the surface edge of air– from step I_n to E_{InT} –, (*ii*) extract the granular bed-air interface –step P_n–, and (*iv*) identify the surface of the granular bed –steps E_{PnDT} and R_n–. The first main step is applied only to the first image because the location of the drum circumference in common for all images. The three next steps are automatically applied to each of the 10918 recorded images.

A key parameter of this procedure is the choice of the threshold value for binarization. **Fig. 4** illustrates the internal sections of the drum. The granular material is placed between the two glass discs, in the green zone, which corresponds rigorously to the drum cylinder. The camera focus is adjusted to the front face of the drum cylinder – on the right of the green zone in **Fig. 4**a–. Therefore, the projection of the granular bed appears obviously in the direct lighting zone (white), also in the projections of the drum side surface (green), of the ring-shaped guide (yellow), and of the clamping ring (red), **Fig. 4**b. Thus, in order to consider all the powder, including those appearing in the gray region (**Fig. 4**c), the threshold value should be lower than the peaks in the histogram corresponding to the white and gray zones (**Fig. 4**d). The peripheral part of the profile (in the gray zone) is here far from linearity and it appears to be the zone where the profile changes shape most significantly during rotation –between avalanches–; so this part includes an important information to describe the granular bed movement and to distinguish the behaviors.

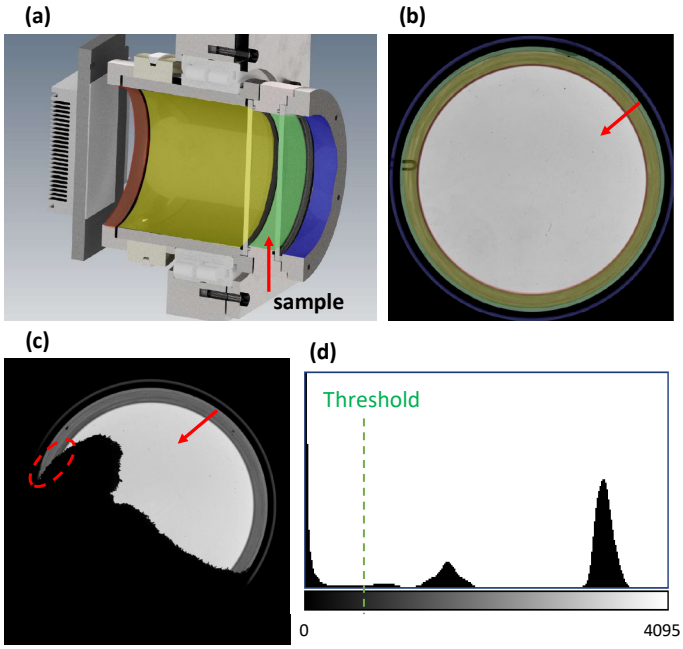

Fig. 4. Focus on the rotating unit. (a) Side cut; the internal surface of each part is colorized to distinguish them. (b) Cross view; colorization using the same colors. (c) Typical image of spruce powder (shadow). (d) Histogram showing the pixel frequency of the gray levels (black (value = 0); white (value = 4095)).

3 Flowability Descriptors

Several descriptors can be determined from individual avalanche events, including Upper Angle of Stability (UAS), Lower Angle of Stability (LAS), avalanche size (UAS-LAS) [27], the time between avalanches and their duration [28], and the energy associated with avalanches [12]. These descriptors give information about the dynamics of the flowing material, but require precise identification of each event; it is challenging to automate this process for the highly cohesive granular materials due to a continuum in amplitude from microscopic events –involving some grains– to the macroscopic events –modifying the whole profile–. Moreover, the identification of events become more and more difficult as the cohesiveness decreases, and the choice of the threshold value to isolate the relevant events is arbitrary. Consequently, this approach is tedious both to granular material presenting a high or poor flowability. Other flowability descriptors are determined from the overall flow, considering continuous measurements –during events and between successive events–.

The **cohesive index (CI)** gives an overview of the temporal fluctuations of the granular bed-air interface (illustrated by **Fig. 5**). The standard deviation, denoted as σ(*x*), is calculated for each abscissa value (*x*) by comparing the series of interface positions $y_i(x)$ over time to the average interface position $\bar{y}(x)$ (Eq. 1),

$$\sigma(x) = \sqrt{\frac{\sum_{i=1}^{N_y(x)} \left(\bar{y}(x) - y_i(x,t)\right)^2}{N_y(x)}} \qquad (1)$$

where $N_y(x)$ is the number of interface pixel ordinates y_i at the abscissa x. The cohesive index (CI) is then obtained by averaging these standard deviations across the entire interface (Eq. 2),

$$\mathrm{CI} = \frac{1}{D_{crop}} \sum_x \sigma(x) \quad (2)$$

where D_{crop} is the cropped diameter, meaning the amplitude in abscissa on which the calculation is applied. We can notice that CI requires prior calculation of the average interface position $\bar{y}$, which is possible for a given abscissa if it belongs to the intersection of the abscissa intervals for all the profiles over time (Eq. 3).

$$D_{crop} = \min(x_{max,i}) - \max(x_{min,i}) \quad (3)$$

Therefore, the profile ends are frequently excluded from the calculation of CI.

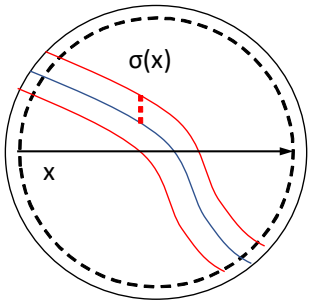

Fig. 5. Interface fluctuations considered for the calculation of the Cohesive index *CI*.

Interaction forces acting between grains (Van der Waals, capillary, electrostatic, and magnetic interactions) create temporal flow fluctuations. CI has the benefit of directly depending on the total cohesive forces.

Previous researches have shown the effectiveness of this flowability descriptor [29,30], so it will be a valuable reference for evaluating and challenging other descriptors in this work.

The **irregularity of the surface profile (r^2)** indicates how linear the granular surface is while rotating in the drum. Linear Regression (LR) is a commonly used method in literature to calculate r^2 according to Eq. (4).

$$r^2 = 1 - \frac{\sum_{i=1}^{N} (\hat{y}_i - y_i)^2}{\sum_{i=1}^{N} (y_i - \bar{y})^2} \quad (4)$$

Its value is as close to 1 as the cumulative vertical distance between the profile and the regression line (Eq. 5) is low.

$$\hat{y}_i = A\, x_i + B \quad (5)$$

The results of r^2 (LR) are influenced by the rotation of the powder, even if the shape of the interface does not change, because the vertical distances between experimental points (x_i, y_i) and the point belonging to the fitting line $(x_i, \hat{y}_i)$ are not constant when the drum rotates (**Fig. 6**). To overcome this limitation, Principal Component Regression (PCR), based on Principal Component Analysis (PCA) in one direction, is introduced as a method for fitting the profile in a rotating drum and calculating r^2 (Eq. 6).

$$r^2 = 1 - \frac{\sum_{i=1}^{N}(d_i)^2}{\sum_{i=1}^{N}[(y_i-\bar{y})^2+(x_i-\bar{x})^2]} \tag{6}$$

$$\begin{cases} \hat{y}'_i = A'\,x_i + B' \Leftrightarrow \hat{x}'_i = \dfrac{y_i}{A'} - \dfrac{B'}{A'} \\ d_i = \dfrac{|A'\,x_i - y_i + B'|}{\sqrt{A'^2+1}} = \dfrac{|\hat{y}'_i - y_i|}{\sqrt{A'^2+1}} = \dfrac{|\hat{x}'_i - x_i|}{\sqrt{\left(1/A'\right)^2+1}} \end{cases} \tag{7}$$

The regression line and the experimental points are offset by a minimum distance, or Euclidean distance, which is d_i (Eq. 7). Consequently, PCR demonstrates a mathematical independence from variations due to drum rotation, making it a robust method for analyzing surface irregularity in rotating drum experiments.

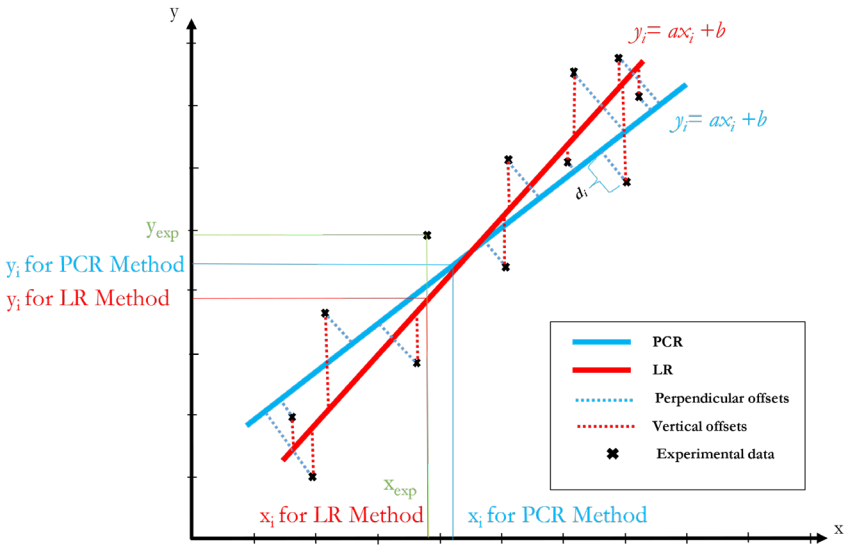

Fig. 6. The difference between LR and PCR methods for calculating the surface profile irregularity (r^2).

Angular descriptors play a significant role in describing the flow behavior of granular materials within a rotating drum (**Fig. 7**). One such descriptor is the **Dynamic Angle of Repose (AoR, θ),** which describes the angle formed by the granular material as it rotates [31]. More precisely, it is the surface angle that lies between the linear fit of the material interface –now through PCR– and the horizontal line (blue angle). Another important angular descriptor is the centroid angle [32]. The **centroid angle**, α, is commonly defined as the angle that the horizontal line made with the line connecting the center of the drum (x_D, y_D) to the center of mass of the bulk(x_{nR}, y_{nR}) (green angle). In the case of non-cohesive powders with flat profiles, |α - θ| was observed to be 90 degrees. In order to have consistency between the centroid angle and the surface angle, we introduced **β** instead of α, defined as the angle between the vertical line and the line connecting the center of the drum to the bulk powder's center of mass (red angle). In the case of cohesive powder, the profile is neither flat nor symmetrical during rotation, and the values of β and θ are different. Therefore, we propose a new descriptor, defined as the **absolute difference between the centroid angle and the angle of repose |β - θ|**, to capture variations in the profile shape.

(a) (b)

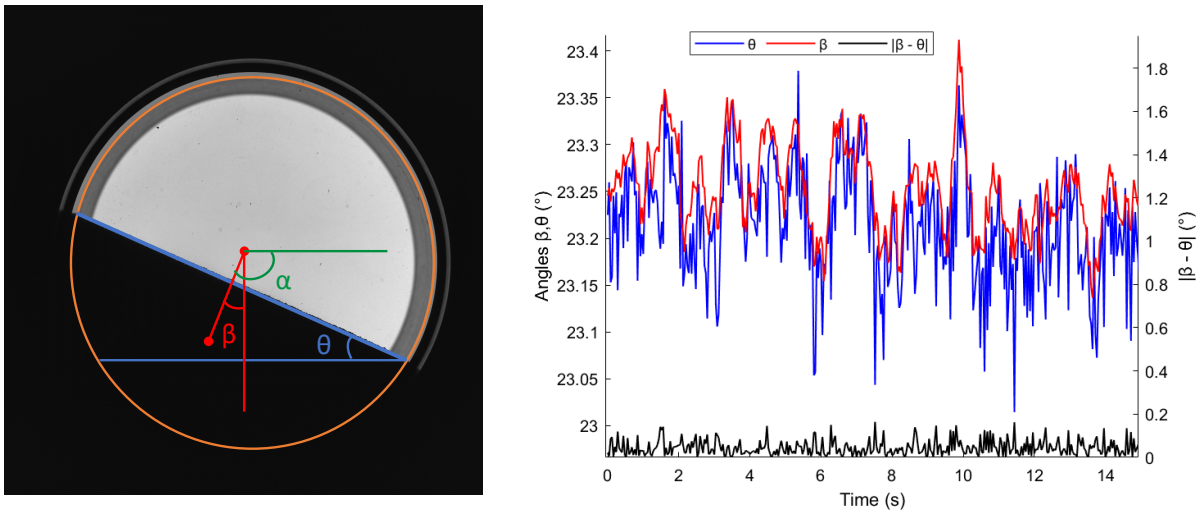

Fig. 7. (a) Geometric definition of the angular descriptors, case of glass beads in the drum. (b) Variation of the angular descriptors while rotating.

The **area** of the granular material projection in the rotating drum is determined through the total number of white pixels (value = 1) in the binary image representation R_n (see **Fig. 3**), using the "*bwarea*" function. For a better representation of this descriptor, the previous value is divided by the number of pixels corresponding to the empty drum, computed from the binarized F_{DT} image. The area is thus expressed as a percentage of drum volume occupied by the granular bed.

Another indicator is the **profile peak** y_{max} that refers to the ordinate of the highest point in the granular material profile P_n (**Fig. 3**). To avoid any effect of camera vertical translation or zoom/unzoom from one test to another, the absolute value of y_{max} is compared to the ordinate of the drum centroid y_D and this difference is multiplied by the pixel size, in centimeter.

As the granular material flows in the drum, descriptor values fluctuate over time. Commonly, the average values of descriptors are used to compare the behavior of one granular material to another. It is also interesting to note that the amplitude of the fluctuations of these descriptors is different among different materials during drum rotation. **Fig. 8** represents the graph of centroid angle evolution during the rotation of glass beads and spruce powder. We recognize how other than the fact that spruce has higher average centroid angle $\bar{\beta}$ than that of glass, also its standard deviation σ(β) is greater. It is reasonable to ask whether the standard deviations of some of these descriptors might also be relevant for distinguishing granular materials from the flowability point of view. That is why both the **average value** and the **standard deviation** for each descriptor through rotating time were calculated; except for CI which intrinsically corresponds to the spatial average of the temporal standard deviations of the profile's local position.

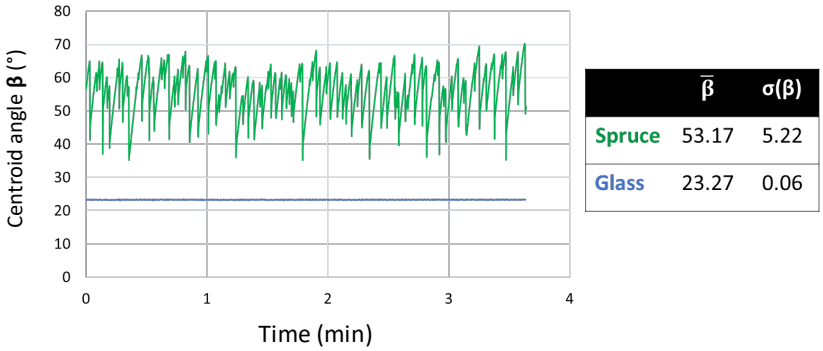

	$\bar{\beta}$	σ(β)
Spruce	53.17	5.22
Glass	23.27	0.06

Fig. 8. Difference of centroid angle values between glass beads and spruce powder.

3.1 Qualitative analysis of flow behaviors

Different flow behaviors of granular materials among the ones depicted in the literature [25] were visually identified by the qualitative analysis of the rotating drum tests (**Fig. 9**). A rolling regime was recognized for the glass beads, through a continuous flow and an extremely smooth and linear profile. Very small avalanches started to appear with zinc powder and sand, with zinc remaining in the rolling regime while sand exhibiting slumping behavior. Sand might experience higher interparticle interactions than glass or zinc, leading to bed slumping. Finally, poplar and spruce powders flow according to a cascading regime, exhibiting significant disruption to their behavior, characterized by far more noticeable avalanches: clumps of powder develop, fall and disintegrate along the free surface, resembling the block-movement-based dynamics described by T. Kronlachner et al. [33].

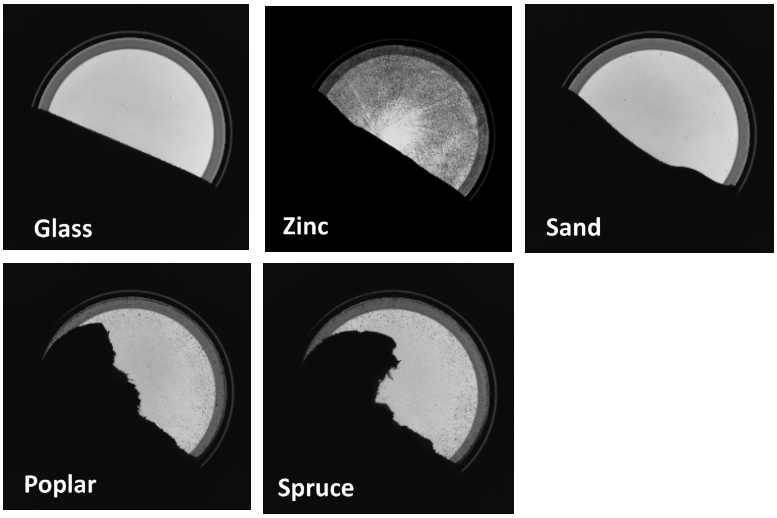

Fig. 9. Example of images of the different material rotating inside the drum.

3.2 Comparative evaluation of the performance of flow descriptors

To proceed with a quantitative assessment of the flowability, we examined a number of flowability descriptors. The following section provides a thorough analysis of these descriptors for each type of granular material.

The results of the cohesive index (CI) are illustrated in **Fig. 10**. Spruce and poplar powders show high overall surface fluctuation –represented by σ(x)–, whereas sand has lower fluctuations compared to the wood powders, but higher than zinc and glass beads. Glass beads nearly do not experience surface fluctuations, as they consistently roll down in a steady manner.

Consequently, according to increasing CI values –which normalize σ(x) along the profile (Eq. 2) – granular materials are ordered as follow: glass, zinc, sand, poplar and spruce. These findings align well with the qualitative observations of each material's profile. This alignment between qualitative (**Fig. 9**) and quantitative (**Fig. 10**) analyses supports the use of the cohesive index as a basis for evaluating other flowability descriptors in our study. CI and flowability being negatively correlated, we can thus consider that glass beads have the highest flowability, followed by zinc, sand, poplar, and finally spruce with the poorest flowability.

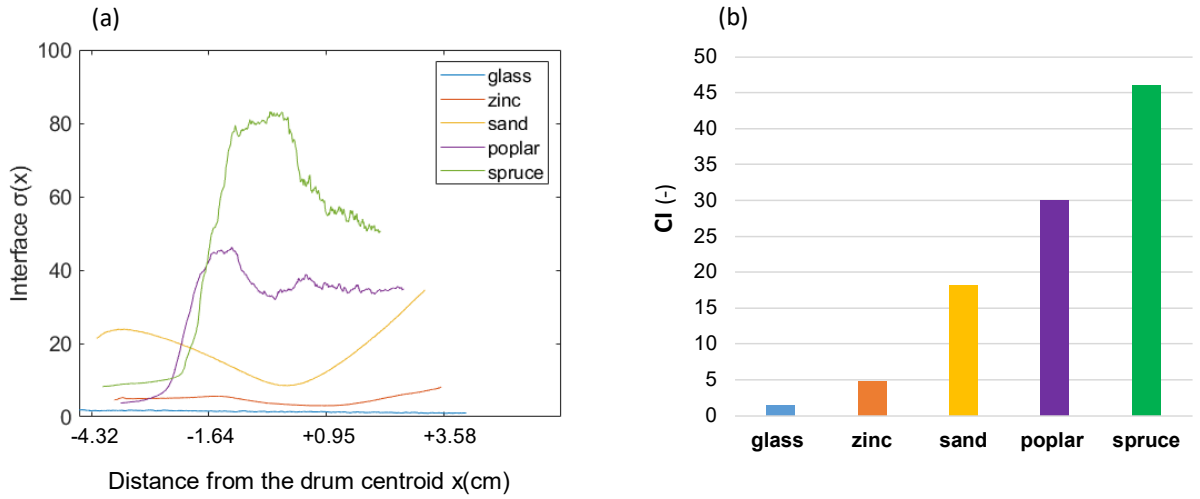

Fig. 10. (a). The interface fluctuation σ(*x*) of the different materials along the profile with respect to the drum centroid. (b). Their respective cohesive indexes (CI).

All the other flowability descriptors mentioned in the previous section were calculated and presented in **Fig. 11** and **Table 2**.

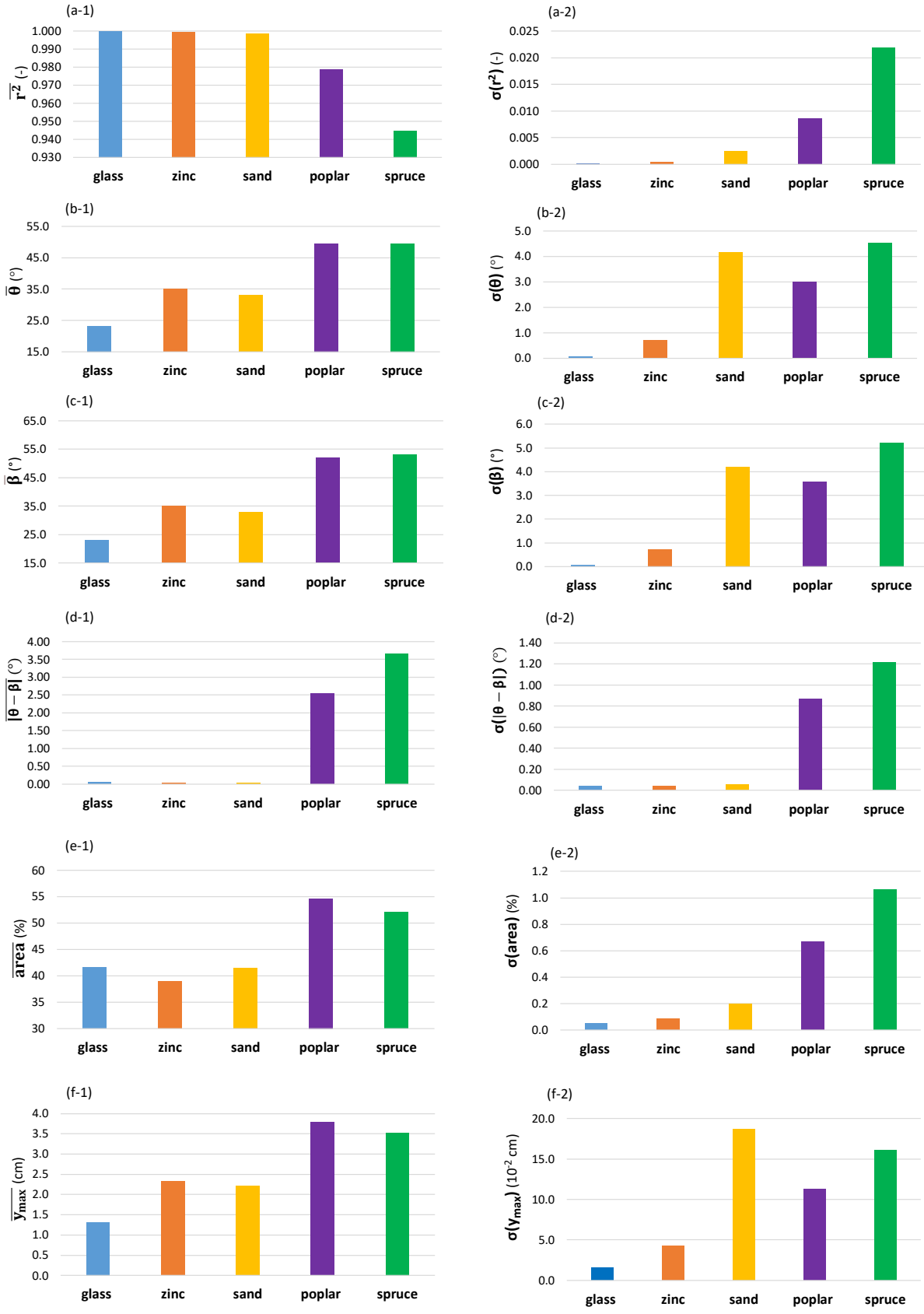

Fig. 11. Values of the flow descriptors tested for all granular materials.

Table 2: Values of the flowability descriptors for the granular materials. The value ranking ((I) to (V)) is reported in round brackets. The red font is used when the value rank differs from the one of CI used as reference, while the green font is used when the value ranking of the description is identical to the one of CI.

	Glass	Zinc	Sand	Poplar	Spruce
CI Decreasing value ranking =increasing flowability	1.438 (*V*)	4.768 (*IV*)	18.167 (*III*)	30.033 (*II*)	45.939 (*I*)
$\overline{r^2}$ Increasing value ranking	0.9999 (*V*)	0.9994 (*IV*)	0.9986 (*III*)	0.9786 (*II*)	0.9448 (*I*)
$\sigma(r^2)$ Decreasing value ranking	0.000019 (*V*)	0.000450 (*IV*)	0.002399 (*III*)	0.0086 (*II*)	0.021957 (*I*)
$\bar{\theta}$ (°) Decreasing value ranking	23.226 (*V*)	35.035 (*III*)	32.984 (*IV*)	49.481 (*II*)	49.522 (*I*)
$\sigma(\theta)$ (°) Decreasing value ranking	0.074 (*V*)	0.719 (*IV*)	4.182 (*II*)	3.010 (*III*)	4.540 (*I*)
$\bar{\beta}$ (°) Decreasing value ranking	23.268 (*V*)	34.999 (*III*)	32.945 (*IV*)	52.005 (*II*)	53.166 (*I*)
$\sigma(\beta)$ (°) Decreasing value ranking	0.061 (*V*)	0.732 (*IV*)	4.208 (*II*)	3.585 (*III*)	5.220 (*I*)
$\overline{\lvert\beta-\theta\rvert}$ (°) Decreasing order	0.042 (*III*)	0.036 (*V*)	0.039 (*IV*)	2.524 (*II*)	3.644 (*I*)
$\sigma(\lvert\beta-\theta\rvert)$ (°) Decreasing value ranking	0.04162 (*V*)	0.04224 (*IV*)	0.06050 (*III*)	0.86670 (*II*)	1.21547 (*I*)
$\overline{Area}$ (%) Decreasing value ranking	41.576341 (*III*)	38.94993 (*V*)	41.43592 (IV)	54.59984467 (*I*)	52.08129786 (*II*)
$\sigma(Area)$ (%) Decreasing value ranking	0.0526878 (*V*)	0.081788 (*IV*)	0.193965 (*III*)	0.666973838 (*II*)	1.064214422 (*I*)
$\overline{y_{max}}$ (cm) Decreasing value ranking	1.323 (*V*)	2.321 (*III*)	2.209 (*IV*)	3.789 (*I*)	3.527 (*II*)
$\sigma(y_{max})$ (10^{-2} cm) Decreasing value ranking	1.606 (*V*)	4.208 (*IV*)	18.706 (*I*)	11.341 (*III*)	16.113 (*II*)

The qualitative analysis of the granular material profiles suggests that profile linearity increases with flowability. The profile is smoother and more linear for glass, zinc, and sand, whereas poplar and spruce exhibit irregular profile shapes. The average value $\overline{r^2}$ (from Principal Component Regression) decreases in the following order (**Fig. 11**, a-1, **Fig. 12** and **Table 2**): glass, zinc, sand, poplar, then spruce. This is consistent with CI results and may serve as a relevant flowability descriptor.

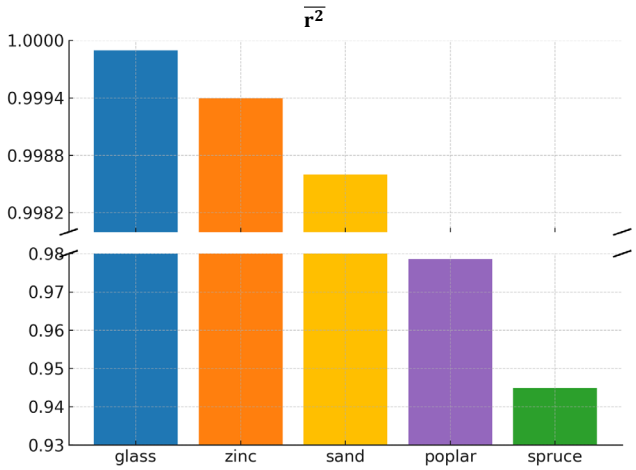

Fig. 12. Clearer view of the $\overline{r^2}$ values using a cropped y-axis graph.

When the flowability increases, the edge effect of the drum lateral inner wall on the granular material decreases in comparison with the gravitational effect. It could be expected that both $\overline{\theta}$ and $\overline{\beta}$ to decrease as the flowability increases –a perfect flowability would lead to zero angles–. But the results reveal that the granular material classification according to these descriptors is not consistent with that using CI: the order of zinc and sand is inverted, and the values of poplar and spruce are very close (**Fig. 11**, b-1, c-1 and **Table 2**). $\overline{\theta}$, $\overline{\beta}$ are not reliable descriptors for flowability.

Due to their geometric definition, the values of θ and β are equal if the profile is flat or symmetrical –*i.e*. if the granular material have a high flowability–. Thus, the angular difference $\overline{|\beta - \theta|}$ is expected to decrease as the flowability increases. The value of this descriptor is approximately null for glass, zinc, and sand. To be more detailed, $\overline{|\beta - \theta|}$ for zinc (0.036) is less than that for sand (0.039), which is further less than that for glass (0.042). On the other hand, $\overline{|\beta - \theta|}$ increases for poplar and spruce where the profile is more irregular and the angles are more distinct. Thus, $\overline{|\beta - \theta|}$ appears to be a promising descriptor to classify the granular materials presenting a poor flowability but it is not applicable to granular materials presenting a high flowability. It is not a very versatile descriptor for a broad range of flowability.

The stronger the interparticle forces, the lower the flowability. Yet, when the drum rotates, powder aeration is the result of a balance between these interparticle forces and gravitational forces, and increases the bulk volume of the granular bed. A correlation between granular bed projection area and flowability can be expected. The $\overline{\text{area}}$ of the inorganic materials (glass, zinc, sand) is less than that of the organic materials (poplar, spruce) (**Fig. 10**, e-1). Nonetheless, $\overline{\text{area}}$ does not sort the different granular materials as classified by CI. Some factors influencing powder aeration do not appear to be correlated with flowability. Hence it cannot act as a consistent flow descriptor.

The cohesiveness of the powder leads to an increase in the period between two successive avalanches. Thus, if powder flowability is low, the profile is likely to reach a higher elevation, y_{max}. The average value $\overline{y_{max}}$ does not classify the granular materials in the same way as CI (**Fig. 11**, f-1). Consequently, both $\overline{y_{max}}$ and $\sigma(y_{max})$ cannot be considered as appropriate flowability descriptors.

In the rotating drum, the behavior of a granular material presenting a high flowability exhibits a continuous flow, whereas the more irregular the profile, the greater the avalanche amplitude and period. Thus, the relevant descriptors based on the standard deviation are supposed to return a lower value the higher the flowability of the granular material.

The standard deviation $\sigma(r^2)$ increases for the same order of materials (**Fig. 11**, a-2). Consequently, this descriptor is consistent with CI.

The standard deviations σ(θ) and σ(β) increase in the following order: glass, zinc, poplar, sand, and spruce (**Fig. 11**, b-2, c-2). The ranking of the granular materials flowability is not consistent with the CI results. The values of σ(θ) and σ(β) for sand –higher than the ones for poplar– were initially surprising because sand showed relatively good flowability. However, after analyzing the images, the sand was slumping downwards such that the whole bed was moving approximately each 3 seconds which created significant fluctuations in the angles' values (**Fig. 13**). Slumping is not necessarily correlated to a poor flowability. These descriptors are thus sensitive to the flowing regime. Therefore, σ(θ) and σ(β) cannot be used as robust flowability descriptors for granular materials exhibiting a high diversity in flow behaviors.

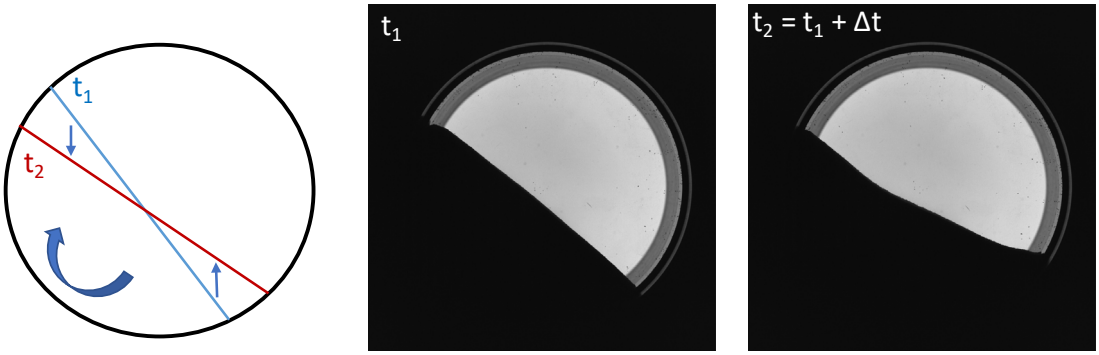

Fig. 13. Dynamic behavior of the sand inside the rotating drum at different time instants (t_1, t_2).

Fig. 14 shows that the standard deviation σ(|β − θ|) values rise following the order of glass, zinc, sand, poplar, and finally spruce. This proves that σ(|β − θ|) is a suitable flowability descriptor.

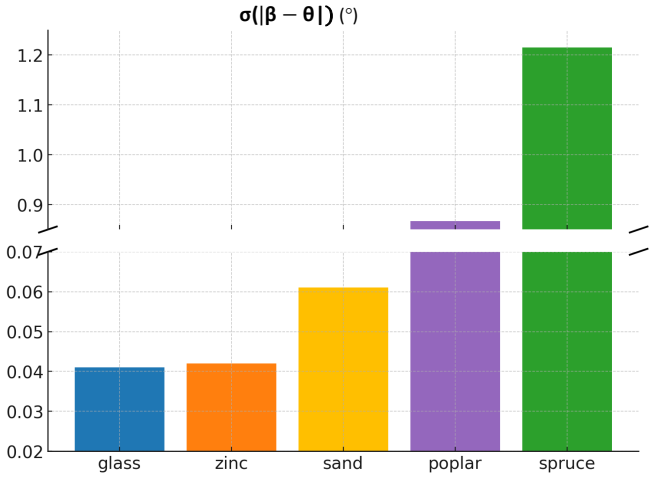

Fig. 14. Clearer view of the σ(|β − θ|) values using a cropped y-axis graph.

The fluctuations in the projected granular material area in a rotating drum during rotation are likely to arise for several reasons related to the dynamic behavior of the material and drum rotation. As the drum rotates, avalanches may form where the particles roll down from top layers to modify the bed packing arrangement and density, causing fluctuations in the area. The standard

deviation σ(area) is insignificant for glass and zinc, low for sand, and quite remarkable for the wood species where spruce has the highest value. So σ(area) follows the same order as CI (**Fig. 11**, e-2). Thus, σ(area) is a good descriptor in studying the materials' flowability.

The standard deviation $\sigma(y_{max})$ of the sand is the highest due to the sliding of the powder bed, which leads to big variations in the y_{max} reached over time (**Fig. 11**, f-2).

4 Conclusion

The study of granular material flowability in a rotating drum has provided significant insights into their flow behavior under unconfined conditions. Different granular materials from strong to poor cohesion were selected. A rigorous experimental procedure was implemented to obtain a quasi-static regime independently of the initial conditions. The image processing took into account the whole profile. Several flowability descriptors based on the whole surface profile, on the surface and volume angles were calculated. It was then possible to assess the ability of these descriptors to classify these powders according to their highly variable flow behavior. The ranking obtained for each descriptor value was compared with that of the cohesive index (CI) used as a benchmark for evaluation.

The results showed that some descriptors are sensitive to other features rather than just being based on the granular material flowability. These features include the interaction between the material and the cylinder drum wall due to friction, and the bed packing that is influenced by the particles size, shape, and bulk density. However, other flowability descriptors depend primarily on the material intrinsic properties regarding the interaction between the particles as the cohesive and attractive forces. Therefore, CI, $\overline{r^2}$, $\sigma(r^2)$, $\sigma(|\theta - \beta|)$ and σ(area) are found to be the most efficient flowability descriptors. These descriptors demonstrated reliability and consistency, thus, one could confidently recommend to use them in future studies and practical applications. Moreover, contrary to CI, it is important to note than the four last descriptors are compute over the whole profile, including the peripheral parts, where the profile is far from linearity and where it changes shape most significantly during rotation. Among them, σ(area) appears to be more robust against the inaccuracies of image capture and processing since it is based on the whole projection of the granular bed in the drum. Consequently, inaccuracy in the description of the free surface –*e.g.* a change in the profile due to the threshold value– will have a more moderate impact on the value of this descriptor. Such findings could bring improvement in the understanding of powder behavior under low stress conditions and will be of vital use for processes optimization, helping to raise the efficiency of production lines.

The flow behavior of the granular material will surely be impacted by the drum conditions like wall friction and speed [9], and consequently the values of the flowability descriptors will change. However, the interest is whether the classification of the different materials remains the same, and this question requires further investigation. Moreover, developing a deeper physical understanding of how particle properties—such as size, shape, friction, and cohesive interactions—affect flow descriptors is our further step. Future research will focus on correlating the physicochemical properties of particles with the granular materials' flowability descriptors, enabling a more comprehensive understanding of their flow dynamics while determining a representative simulation model.

Acknowledgments

The authors would like to acknowledge the French Ministry of Higher Education and Research for their financial support.

References

[1] M. PELEG, FLOWABILITY OF FOOD POWDERS AND METHODS FOR ITS EVALUATION, (n.d.). https://doi.org/10.1111/j.1745-4530.1977.tb00188.x.
[2] C. Salameh, J. Scher, J. Petit, C. Gaiani, C. Hosri, S. Banon, Physico-chemical and rheological properties of Lebanese kishk powder, a dried fermented milk-cereal mixture, Powder Technol. 292 (2016) 307–313. https://doi.org/10.1016/j.powtec.2016.01.040.
[3] J. Xiang, L. Liu, X. Cui, Y. He, G. Zheng, C. Shi, Effect of Fuller-fine sand on rheological, drying shrinkage, and microstructural properties of metakaolin-based geopolymer grouting materials, Cem. Concr. Compos. 104 (2019) 103381. https://doi.org/10.1016/j.cemconcomp.2019.103381.
[4] D.S. Shah, K.K. Moravkar, D.K. Jha, V. Lonkar, P.D. Amin, S.S. Chalikwar, A concise summary of powder processing methodologies for flow enhancement, Heliyon 9 (2023) e16498. https://doi.org/10.1016/j.heliyon.2023.e16498.
[5] J. Yang, T. Bell, M. Pasha, Evaluation of a Uniaxial Powder Tester and Comparison with an Annular Shear Tester, Powder Technol. 403 (2022) 117405. https://doi.org/10.1016/j.powtec.2022.117405.
[6] J. Zegzulka, D. Gelnar, L. Jezerska, R. Prokes, J. Rozbroj, Characterization and flowability methods for metal powders, Sci. Rep. 10 (2020) 21004. https://doi.org/10.1038/s41598-020-77974-3.
[7] D18 Committee, Test Method for Bulk Solids Using Schulze Ring Shear Tester, (n.d.). https://doi.org/10.1520/D6773-16.
[8] B.H. Kaye, J. Gratton-Liimatainen, N. Faddis, Studying the Avalanching Behaviour of a Powder in a Rotating Disc, Part. Part. Syst. Charact. 12 (1995) 232–236. https://doi.org/10.1002/ppsc.19950120505.
[9] C.-Y. Hung, C.P. Stark, H. Capart, Granular flow regimes in rotating drums from depth-integrated theory, Phys. Rev. E 93 (2016) 030902. https://doi.org/10.1103/PhysRevE.93.030902.
[10] E.R.L. Espiritu, A. Kumar, A. Nommeots-Nomm, J.A.M. Lerma, M. Brochu, Investigation of the rotating drum technique to characterise powder flow in controlled and low pressure environments, Powder Technol. 366 (2020) 925–937. https://doi.org/10.1016/j.powtec.2020.03.029.
[11] W.B. Lee, E. Widjaja, P.W.S. Heng, L.W. Chan, Investigating the effect and mechanism of particle size distribution variability on mixing using avalanche testing and multivariate modelling, Int. J. Pharm. 563 (2019) 9–20. https://doi.org/10.1016/j.ijpharm.2019.03.045.
[12] Ž. Trpělková, H. Hurychová, M. Kuentz, B. Vraníková, Z. Šklubalová, Introduction of the energy to break an avalanche as a promising parameter for powder flowability prediction, Powder Technol. 375 (2020) 33–41. https://doi.org/10.1016/j.powtec.2020.07.095.
[13] V.R. Nalluri, M. Kuentz, Flowability characterisation of drug-excipient blends using a novel powder avalanching method, Eur. J. Pharm. Biopharm. Off. J. Arbeitsgemeinschaft Pharm. Verfahrenstechnik EV 74 (2010) 388–396. https://doi.org/10.1016/j.ejpb.2009.09.010.
[14] H. Yang, R. Li, P. Kong, Q.C. Sun, M.J. Biggs, V. Zivkovic, Avalanche dynamics of granular materials under the slumping regime in a rotating drum as revealed by speckle visibility spectroscopy, Phys. Rev. E 91 (2015) 042206. https://doi.org/10.1103/PhysRevE.91.042206.
[15] H.P. Goh, P.W.S. Heng, C.V. Liew, Comparative evaluation of powder flow parameters with reference to particle size and shape, Int. J. Pharm. 547 (2018) 133–141. https://doi.org/10.1016/j.ijpharm.2018.05.059.

[16] W.B. Lee, E. Widjaja, P.W.S. Heng, L.W. Chan, The effect of rotation speed and particle size distribution variability on mixability: An avalanche rheological and multivariate image analytical approach, Int. J. Pharm. 579 (2020) 119128. https://doi.org/10.1016/j.ijpharm.2020.119128.
[17] M. Kuentz, P. Schirg, Powder flow in an automated uniaxial tester and an annular shear cell: a study of pharmaceutical excipients and analytical data comparison, Drug Dev. Ind. Pharm. 39 (2013) 1476–1483. https://doi.org/10.3109/03639045.2012.728228.
[18] F. Boschini, V. Delaval, K. Traina, N. Vandewalle, G. Lumay, Linking flowability and granulometry of lactose powders, Int. J. Pharm. 494 (2015) 312–320. https://doi.org/10.1016/j.ijpharm.2015.08.030.
[19] G. Lumay, F. Boschini, K. Traina, S. Bontempi, J.-C. Remy, R. Cloots, N. Vandewalle, Measuring the flowing properties of powders and grains, Powder Technol. 224 (2012) 19–27. https://doi.org/10.1016/j.powtec.2012.02.015.
[20] P. Janssen, A. Neveu, G. Lumay, The flowability of lactose powders to optimize tableting processes, ONdrugDelivery (2020) 58–63.
[21] A. Faqih, B. Chaudhuri, A.W. Alexander, C. Davies, F.J. Muzzio, M. Silvina Tomassone, An experimental/computational approach for examining unconfined cohesive powder flow, Int. J. Pharm. 324 (2006) 116–127. https://doi.org/10.1016/j.ijpharm.2006.05.067.
[22] A. Alexander, B. Chaudhuri, A. Faqih, F. Muzzio, C. Davies, M. Tomassone, Avalanching flow of cohesive powders, Powder Technol. 164 (2006) 13–21. https://doi.org/10.1016/j.powtec.2006.01.017.
[23] J.J. Fitzpatrick, T. Iqbal, C. Delaney, T. Twomey, M.K. Keogh, Effect of powder properties and storage conditions on the flowability of milk powders with different fat contents, J. Food Eng. 64 (2004) 435–444. https://doi.org/10.1016/j.jfoodeng.2003.11.011.
[24] P. Tegzes, T. Vicsek, P. Schiffer, Development of correlations in the dynamics of wet granular avalanches, Phys. Rev. E 67 (2003) 051303. https://doi.org/10.1103/PhysRevE.67.051303.
[25] J. Mellmann, The transverse motion of solids in rotating cylinders—forms of motion and transition behavior, Powder Technol. 118 (2001) 251–270. https://doi.org/10.1016/S0032-5910(00)00402-2.
[26] M. Wojtkowski, O.I. Imole, M. Ramaioli, E.C. Montes, S. Luding, Behavior of Cohesive Powder in Rotating Drums, (n.d.).
[27] M. Quintanilla, J. Valverde, A. Castellanos, The transitional behaviour of avalanches in cohesive granular materials, J. Stat. Mech. Theory Exp. 2006 (2006) P07015. https://doi.org/10.1088/1742-5468/2006/07/P07015.
[28] Y.S. Lee, R. Poynter, F. Podczeck, J.M. Newton, Development of a dual approach to assess powder flow from avalanching behavior, AAPS PharmSciTech 1 (2000) E21. https://doi.org/10.1208/pt010321.
[29] A. Neveu, F. Francqui, G. Lumay, Measuring powder flow properties in a rotating drum, Measurement 200 (2022) 111548. https://doi.org/10.1016/j.measurement.2022.111548.
[30] N. Preud'homme, G. Lumay, N. Vandewalle, E. Opsomer, Numerical measurement of flow fluctuations to quantify cohesion in granular materials, Phys. Rev. E 104 (2021) 064901. https://doi.org/10.1103/PhysRevE.104.064901.
[31] N.-S. Cheng, K. Zhao, Difference between static and dynamic angle of repose of uniform sediment grains, Int. J. Sediment Res. 32 (2017) 149–154. https://doi.org/10.1016/j.ijsrc.2016.09.001.
[32] G.L. Wagner, Granular flow in a Rotating Drum, (2013) 1–29., (n.d.).
[33] T. Kronlachner, S. Pirker, T. Lichtenegger, A block-movement-based analysis for cohesive powders in a rotating drum experiment, Powder Technol. 399 (2022) 117209. https://doi.org/10.1016/j.powtec.2022.117209.